International Journal of Innovative Engineering Applications

Journal homepage: https://dergipark.org.tr/ijiea

INVESTIGATION OF THE EFFECTS OF SMAW PARAMETERS AND SEAWATER TEMPERATURE ON PROPERTIES OF AH36 JOINTS AND THE CHEMICAL COMPOSITION OF SEAWATER

Emre Görgün*[1]

[1]*Sivas Cumhuriyet University, Sivas Technical Sciences Vocational School, Railway Systems Department, 58104 Sivas, Turkey*

Abstract

Original scientific paper

Underwater wet welding (UWW) is a critical technique for repairing offshore structures, underwater pipelines, water transport infrastructure, docks, and harbor equipment. In this study, the mechanical and microstructural properties of AH36 low-carbon steel weldments were investigated using metal arc welding (SMAW), an underwater wet welding method, at various welding current strengths and seawater temperatures. The relationship between changes in seawater temperature and welding current parameters and their impact on seasonal variations in welding conditions and seawater composition was examined. In the first stage, the yield strength of AH36 was statistically modeled using a central composite design with input parameters of seawater temperature (ranging from 9.7 °C to 25.3 °C) and weld current value (ranging from 49A to 90A). Optimal conditions were determined, resulting in a yield strength of 270MPa, achieved at a seawater temperature of 17.5 °C and a weld current value of 69.5 A. In the second stage, data from optimization studies were utilized to develop elemental exchange equations for Cr (R^2=87.3), Ni (R^2=64.45), and Mn (R^2=65.74) ions in seawater. The findings reveal that weld current intensity primarily influences changes in Cr content in seawater, seawater temperature is correlated with Ni content, and both current intensity and seawater temperature affect the Mn content. The analytical techniques employed include Inductively Coupled Plasma Mass Spectrometry (ICP-MS) for seawater ion analysis, Energy Dispersive Spectroscopy (EDS) point analysis to determine the chemical composition of AH36, and Scanning Electron Microscopy (SEM) for microstructural analysis.

Keywords: *Response surface method (RSM), steel plate A36, stick metal arc welding (SMAW), underwater wet welding (UWW), welding current.*

SMAW PARAMETRELERİNİN AH36 BAĞLANTI ÖZELLİKLERİNE VE DENİZ SUYUNUN KİMYASAL BİLEŞİMİNE ETKİSİNİN ARAŞTIRILMASI

Özet

Orijinal bilimsel makale

Sualtı kaynağı (SMAW) açık deniz yapılarının, sualtı boru hatlarının, su taşımacılığı altyapısının, rıhtımların ve liman ekipmanlarının onarımı için kritik bir tekniktir. Bu çalışmada, bir sualtı kaynak yöntemi olan metal ark kaynağı (SMAW) kullanılarak AH36 düşük karbonlu çelik kaynakların mekanik ve mikroyapısal özellikleri çeşitli kaynak akım şiddetleri ve deniz suyu sıcaklıklarında incelenmiştir. Deniz suyu sıcaklığı ve kaynak akımı parametrelerindeki değişimler arasındaki ilişki ve bunların kaynak koşulları ve deniz suyu bileşimindeki mevsimsel değişimler üzerindeki etkisi incelenmiştir. İlk aşamada, AH36'nın akma dayanımı, deniz suyu sıcaklığı (9,7 °C ila 25,3 °C arasında değişen) ve kaynak akımı değeri (49A ila 90A arasında değişen) girdi parametreleri ile merkezi bir kompozit tasarım kullanılarak istatistiksel olarak modellenmiştir. Optimum koşullar belirlenmiş ve 17,5 °C deniz suyu sıcaklığı ve 69,5 A kaynak akımı değerinde 270 MPa akma dayanımı elde edilmiştir. İkinci aşamada, optimizasyon çalışmalarından elde edilen veriler deniz suyundaki Cr (R^2=87,3), Ni (R^2=64,45) ve Mn (R^2=65,74) iyonları için element değişim denklemleri geliştirmek için kullanılmıştır. Bulgular, kaynak akım yoğunluğunun öncelikle deniz suyundaki Cr içeriğindeki değişiklikleri etkilediğini, deniz suyu sıcaklığının Ni içeriği ile ilişkili olduğunu ve hem akım yoğunluğunun hem de deniz suyu sıcaklığının Mn içeriğini etkilediğini ortaya koymaktadır. Kullanılan analitik teknikler arasında deniz suyu iyon analizi için İndüktif Eşleşmiş Plazma Kütle Spektrometrisi (ICP-MS), AH36'nın kimyasal bileşimini belirlemek için Enerji Dağılımlı Spektroskopi (EDS) nokta analizi ve mikroyapısal analiz için Taramalı Elektron Mikroskobu (SEM) bulunmaktadır.

Anahtar Kelimeler: *Yanıt yüzey yöntemi (RSM), A36 çelik levha, çubuk metal ark kaynağı (SMAW), sualtı kaynak (UWW), kaynak akımı.*

*Corresponding author.

E-mail address: emregorgun@cumhuriyet.edu.tr (E. Görgün)

Received 12 January 2024; Received in revised form 15 April 2024; Accepted 19 April 2024

 Doi: https://doi.org/10.46460/ijiea.1418641

1 Introduction

Underwater wet welding (UWW) technology has gained widespread recognition owing to its real-time and on-site applications in constructing and maintaining marine structural engineering equipment, including subsea oil pipelines, marine vessel repairs, oil platforms, and offshore turbines [1, 2]. The simplicity of this technology in equipment utilization allows for cost-effective maintenance of complex-shaped structures [3-5]. While shielded metal arc welding (SMAW) remains in use, recent research has shown a growing focus on flux-cored arc welding (FCAW) within the realm of UWW [6-8]. Solid-state friction stir welding has the potential to successfully join steel plates [9-15]. However, it has some shortcomings, such as the requirement of a stirring tool with high-temperature resistance and geometrical limitations. Thus, conventional fusion welding methods, i.e. gas metal arc welding and gas tungsten arc welding, are the most common welding processes used for joining steel parts including stainless steels in various industries [16, 22]. However, these gas shielded arc welding methods cannot be used in under seawater applications. Shielded metal arc welding is particularly valuable for repairing welds that are paramount in deep-water environments [23, 24]. With urbanization and industrialization, industrial chemicals, rare earth elements, platinum group elements (PGE), and radionuclides are increasingly present [25]. This can significantly affect spring water quality, potentially leading to bacterial and pathogenic contamination [26, 27].

Underwater arc welding has been shown in recent studies to be the most suitable method for carrying out repairs and constructing underwater structures. [28]. Nevertheless, several challenges arise when testing welds performed underwater [29]. Among the major difficulties encountered is the rapid contact between the workpiece and water, resulting in a pronounced quenching effect [30]. Hydrogen diffusion occurs due to the dissociation of water, leading to hydrogen-induced cracking, which has been observed to reduce fatigue strength [31]. Arc instability, porosity and loss of alloying elements in welds caused by the presence of infused gases contribute to the deterioration of the mechanical properties and microstructure of the weld metal [32]. In addition, the heat-affected zone (HAZ) is subjected to increased hardness, which can lead to cracking [33]. In order to obtain the required properties in welds, it is recommended to implement control over the input parameters during welding, to include alloying materials in the electrode coating and to use multi-pass welding techniques [34]. There are not many studies in the literature on the environmental effects of weld parameters and their effects on seawater. The main subject of this study is to increase the welding capability and minimise the environmental impact by providing optimum conditions.

This study emphasizes that polluted surface water and groundwater can serve as pathways for various microbiological contaminants, resulting in adverse health effects in humans [35]. Consumption of contaminated drinking water can lead to waterborne diseases, such as diarrhea and gastrointestinal illnesses, responsible for numerous epidemics throughout history [36].

Most studies have discussed the effects of elements on the slag barrier of wet-flux core welding, mainly focusing on molten slag. Welding AH36 presents challenges such as thermal cracking and carbide precipitation, especially in multipass welds, which may lead to alterations in the mechanical strength. Over a century ago, observations were made in the German chrome ore industry, which showed a higher incidence of lung cancer among workers than in the general population. Subsequent investigations revealed that hexavalent chromium (Cr^{6+}) in drinking water was the underlying cause of this elevated risk [37, 39]. Studies underscore the critical significance of Cr content in seawater [40, 41, 42].

This study investigates the environmental impact of welding parameters on seawater during maintenance, repair and manufacturing operations. Thus, it is predicted that the environmental impact of seawater temperature and welding parameters can be minimised.

2 Materials and Methods

2.1 Materials

AH36 steel emerges as a highly favored material within diverse marine sectors, particularly in shipbuilding and underwater structures. The selection of AH36 steel can be attributed to several key factors. Firstly, its high strength is paramount for underwater structures and vessels, offering resilience against water pressure, waves, and environmental stressors, thereby bolstering overall structural integrity. Secondly, its exceptional resistance to corrosion in environments like seawater and high moisture settings significantly prolongs longevity and reduces maintenance costs for underwater structures. Thirdly, AH36 steel shows remarkable toughness even in low-temperature conditions, ensuring reliability and durability in cold water operations. Lastly, its favorable welding properties make it highly suitable for underwater welding processes, facilitating repair and assembly procedures, thereby providing a crucial advantage in underwater applications.

AH36 steel plates with dimensions of 300 mm × 100 mm × 16 mm cut from rolled sheets were used as the base metals. An E7014 electrode with a diameter of 3.25 mm was used as the filler. Welding was performed in a 2000 ml seawater environment, and the chemical compositions of the base metal, filler metal, and seawater are listed in Table 1.

Table 1. Chemical compositions of the base metal, filler metal, and seawater.

Materials	C	Si	Mn	P	S	Al	Ti	Cu	Cr	Ni	Mo	Fe
AH36 (wt%)	0.18	0.50	0.90	0.035	0.035	0.015	0.02	0.35	0.20	0.40	0.08	Bal.
E7014 (wt%)	0.15	0.90	1.25	0.035	0.035	Bal.	Bal.	Bal.	0.20	Bal.	0.30	Bal.
Sea Water (μg/l)	-	200	0.10	40	160	0.7	-	0.5	0.10	0.50	0.10	4

2.2 Welding Procedure

A series of welding experiments using different welding current values and seawater temperatures, using Shielded Metal Arc Welding (SMAW) as the welding method, were conducted in this study. To perform these experiments, a welding machine with a maximum operating capacity of 350 A was used, as recommended in the literature [4]. Before commencing the welding process, all specimens were meticulously prepared. This preparation involved mechanical polishing using abrasive paper to ensure a smooth and uniform surface. Furthermore, chemical cleaning with anhydrous ethanol was conducted to eliminate any dust, oil, or other impurities that could interfere with the welding process or compromise the integrity of the resulting weld joints [3].

The sea water temperature parameters were selected according to the annual changes in sea water temperature according to the data obtained from the Turkish State Meteorological Service. Welding parameters were determined according to TS EN ISO 3834-2 Quality Requirements for Melting of Metallic Materials standard according to electrode diameter, material thickness and material type.

Welding experiments were conducted in a water tank with a water depth of 150 mm. A mechanical arm was used to manipulate the welding electrode to ensure the welding quality. The response surface method was employed to examine the influence of welding current on both the weld and seawater. Optimization experiments using a central composite design (CCD) with the assistance of a Design Expert (13 trial versions) were conducted. Based on the model, the current values tested ranged from 49 to 90 A, and different seawater temperatures ranging from 9.7 °C to 25.3 °C were explored. Subsequently, the multi-response optimization model in MINITAB was used to analyze the concentrations of Cr, Ni, and Mn observed in seawater under optimal experimental conditions [44, 45].

2.3 Microstructure Characterization and Mechanical Performance Test Methods

Samples were prepared according to the EN ISO 17637 standard for visual inspection to determine surface defects and EN ISO 17636-1 standard to determine internal defects [46]. After the plates were welded, the tensile, chemical, and SEM analysis specimens were obtained using the wire-cutting manufacturing method, as shown in Fig. 1. 5 tensile specimens, 5 microscopic characterization specimens and 5 seawater specimens were taken from each test group with a total of 360 specimens for experimental studies.

Fig. 1 illustrates the test specimens' cutting plan and the geometry of tensile test specimens. All the sample areas were chosen from the same position as the weld center. To minimize the impact of random errors on experimental precision, three metallographic specimens and five tensile specimens were selected for each weld parameter [47, 48].

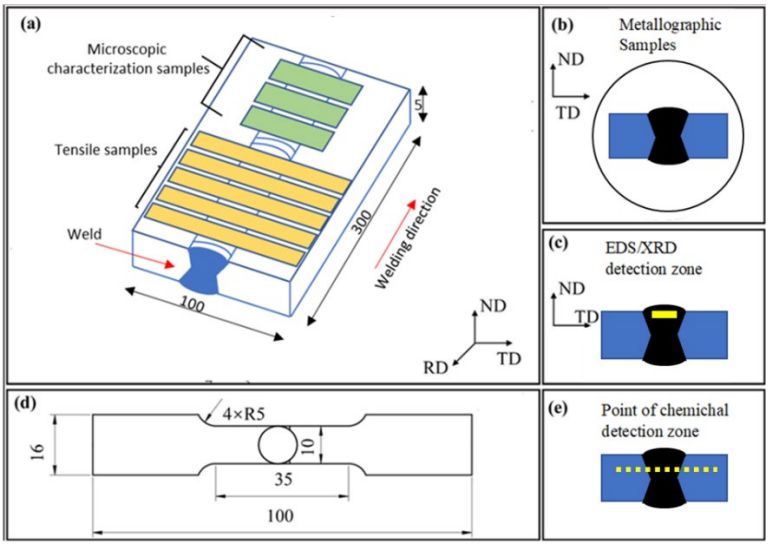

Figure 1. Samples of schematic illustrations of the directions and dimensions (a) location of tensile samples and microscopic characterization samples, (b) metallographic samples, (c) orientation and zone of EDS samples, (d) dimensions of tensile samples, and (e) point locations of chemical test.

To examine the microstructure of the weld metal, particularly the distribution and morphology of the austenite and ferrite phases, a metallographic microscope was employed. The microscope allows for detailed observations and analysis of the internal structure of the weld, providing insights into the arrangement and characteristics of the austenite and ferrite phases. The etching solution consisted of a mixture of hydrochloric and nitric acids.

Electron Backscatter Diffraction (EBSD) was used to analyze the grain size, boundaries, and misorientation of the ferrite and austenite phases. EBSD provides valuable information on the crystallographic properties of materials. Scanning Electron Microscopy (SEM) was used to investigate phase composition and density. The scanning angle ranged from 10° to 80°and the scanning speed was set at 3°/min. The weld joints were characterized in three directions: rolling direction (RD), transverse direction (TD), and average direction (ND). The metallographic, EBSD, and SEM samples were obtained from the surface corresponding to the ND-TD orientation. This allows for consistent analysis and comparison of the weld microstructure and properties in a specific plane [48, 49].

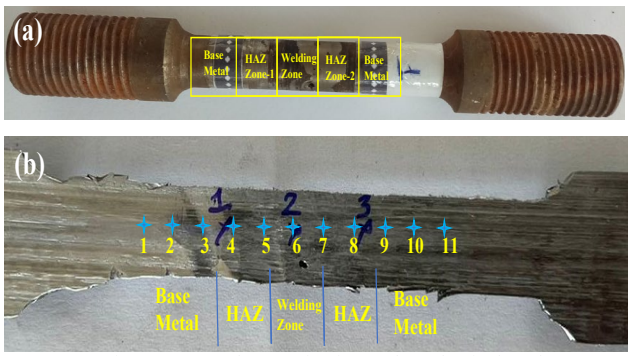

Figure 2. Microstructure characterization and mechanical performance samples (a) samples zones, (b) examination points.

Tensile tests were conducted using an electronic universal testing machine with a maximum load of 15 kN and tensile speed of 2 mm/min, adhering to guidelines from reference documents such as AG-50 kN. The samples were obtained from the specimens shown in Fig. 2(a). To examine the morphology of the tensile fractures, a scanning electron microscope equipped with a tungsten filament was used [56]. Detected spots were systematically distributed, starting from the base metal (BM), extending through the heat-affected zone (HAZ), and culminating at the weld metal center (WM). The spots indicated in Fig. 2(b) were used for microstructural characterization, and the interval between each spot was maintained at 2 mm.

The holes visible in Figure 2(b) are worm holes caused by hydrogen diffusion due to water segregation during welding and are considered acceptable under ISO 5817-Welding - Fusion welded joints in steel, nickel, titanium and their alloys (except beam welding) - Quality levels for defects, but the test was carried out in non-porous areas.

2.4 ICP-MS Performance Test Methods

The welding process was performed with a volume of 2000 ml. seawater medium and 50 ml. Samples were collected from the seawater after each welding. After opening the lids of the containers cooled at room temperature for ICP -MS analysis, the solutions dissolved in Teflon were taken into 50 ml balloon jugs [50, 51]. Dilution was performed by adding 50 ml of ultra-distilled water to the solution, and the samples were placed in plastic tubes. The samples were filtered through 25/0.45 µm filters and stored in a refrigerator at +4 °C until reading. To prevent metal contamination, all the materials used during the dissolution of the samples were passed through HNO3 (1:1) and ultra-distilled water (1/9). An Agilent 7700 series ICP-MS device was used for heavy metal analyses. The study observed the relationship between the variation in Cr and Ni values in seawater and the weld parameters, and meaningful relationships were established [52].

Cr3+ is a micronutrient and an essential nutritional supplement, while Cr6+ is highly toxic to human health. Chromium is an outstanding element in which different species exhibit contrasting behavioral characteristics towards human health (Fig. 6(b)). Cr exists in various oxidation states, from Cr0 to Cr6+. While Cr6+ is often a by-product of industrial contamination, it can also occur naturally in groundwater, depending on the local aquifer geology and water chemistry. This is also necessary to meet regulations in some instances; for example, the allowable limit for Cr6+ in drinking water is 100 ng/ml, as stipulated by the US EPA, whereas the recommended target for Cr6+ by California Public is 0.06 ng/ml [53, 54]. In a recent study conducted by [55], the assessment of environmental risk associated with certain heavy metals, including As, Pb, Cu, Cr, Zn, Mn, Ni, V, Al, and Fe, in the water and sediments of the Bahr El-Baqar drainage was examined. This study emphasized that the ratios of these elements in seawater are essential for evaluating their potential environmental impact.

Among the elements analyzed in this study, Mn, Fe, Cr, Al, and Cu, which have critical importance regarding their effects on the environment and human health, were the focus [56]. To weld in the seawater under different welding conditions, the focus was on establishing a relationship between the presence or absence of elements passing from the welding electrode and the base material into the seawater; thus, trying to find an optimum welding temperature and its effect on seawater was also included in the analysis.

2.5 Multi-Response Optimization Methods

The Response Surface Method (RSM) is a computer-aided mathematical modeling approach distinct from classical optimization methods (REF). This study employed it to identify the optimal experimental outcomes, contingent upon varying the experimental input parameters through the optimization of the experimental conditions. To facilitate this process, the Design Expert 13.00 software package was utilized to ascertain the experiments to be conducted, and the obtained results were subsequently integrated into the program.

RSM combines statistical techniques with mathematical expressions to address problems involving multiple variables. This methodology is widely applicable in various domains, including product formulation, design enhancement, and process development. Central Composite Design (CCD) is an experimental technique used to assess the effects of multiple variables and their interactions. It aims to optimize systems by understanding the impact of different factors on system responses, with applications in various fields such as industrial processes and pharmaceuticals. To accommodate this method, independent variables are scaled to vary between -1 and +1, with the smallest value denoted as -1 and the largest as +1, whereas the midpoint is established as 0. A central composite design encompasses cube points at the corners of a cube, star points outside the cube, and center points at the origin, all of which fall within the -1 to +1 range. The following equation can be mathematically expressed:

$$Y=\beta_0+\Sigma(\beta_i X_i)+\Sigma(\beta_{ii} X_{ii}^2)+\Sigma(\beta_{ij} X_i X_j) \quad (i=1,2,3\ldots..n) \tag{1}$$

where Y is the estimated response variable, n is the number of observations, i and j are linear and quadratic dependent and independent coefficients, respectively, β0 is the constant coefficient, β_i is the linear coefficient, β_{ii} is the interactive coefficient, and β_{ij} is the quadratic

coefficient. In this study, the response variable Y, Yield strength, X1; seawater temperature X2, and spring flow intensity were applied to the model.

3 Results and Discussions

3.1 Microstructure and Elemental Composition

The dynamic nature of seawater composition, the difficulty of analyzing trace element concentrations in seawater with high precision, as well as factors such as environmental conditions, water currents and the general marine ecosystem can change the direct influence of the weld parameters.

Energy-dispersive X-ray spectroscopy (EDS) analysis was used to determine the separation of the Cr-Mn-rich phases. As a result of the EDS analysis, secondary phases rich in Ni, Nb, Cr, and Mo were observed in the Heat Effective Zone (HAZ) region. Fig. 3 (a)-(b).

Subsequently, EDS mapping was employed to determine the elemental distribution along the AH36 weld metal interface. The results obtained are illustrated in Fig. 3(b), (d), and (f). Based on the mapping, it was observed that the elements chromium (Cr) and manganese (Mn) were primarily distributed within the base metal AH36. This suggests that the concentrations of Cr and Mn were relatively higher in the base metal than in the weld metal in this specific analysis.

The EDS mapping analysis revealed that chromium (Cr) was predominantly concentrated within the AH36 base metal. Furthermore, a significant diffusion gradient of Cr was observed across the interface between the base metal and the weld metal. This indicates a notable change in the distribution of Cr as it diffused from the AH36 base metal into the adjacent weld metal. The Cr content of the weld metal was higher than that of the base material. This is consistent with the results of the variation in the line scan analysis. The migration of Al, Si, and S from the base metal to the weld metal affects the properties of the weld metal by changing the composition of the Cr-based filler.

According to the EDS spot analysis results shown in Fig. 3(d), these Nb-rich phases were block-shaped NbC or irregularly shaped Laves phases. The atomic compositions of 2 and 7 are shown in Fig. 3(a), and were found to fulfill the carbide characteristics, proving that carbide formation occurred in the HAZ region.

Phases suitable for A_2B type (A: Ni, Cr, Fe; B: Nb, Mo, Ti) intermetallic compounds are shown in Fig. 3 (a)-(f) 2. According to Dupont, a high chromium (Cr) content tends to enhance the segregation of the Cr-rich phases. This means that when a higher concentration of Cr is present in a material, the Cr-rich phases are more likely to separate or segregate within the structure.

When the carbon content was relatively high, chromium (III) oxide (Cr_2O_3) precipitated. This precipitation occurs when there is an interaction between the high carbon content and the chromium present in the material. The formation of Cr_2O_3 can affect the properties and behavior of the material. In contrast, the leaf phase was formed at a low carbon concentration. As suggested by Ramkumar, the presence of Si and Fe also contributes to the formation of the laves phase [57]. In addition, as shown in Fig. 3(b), a block-shaped white phase rich in Cr and Mn was observed in the AH36 base metal. As shown in Fig. 3(b), the EDS spot analysis results confirmed that the 3,4,5-6 blocky phase was Cr_2O_3.

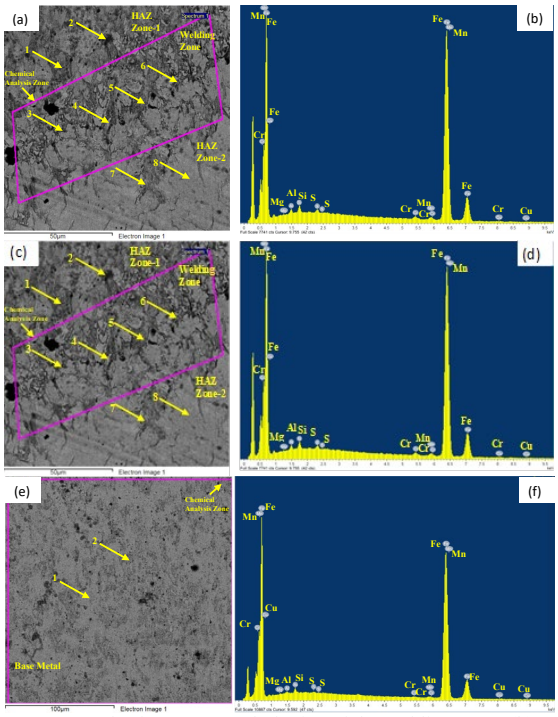

Figure 3. (a) The fracture morphologies of the welding zone, (b) EDS point analysis of the welding zone, (c) the fracture morphologies of the HAZ zone, (d) EDS point analysis of HAZ zone, (e) the fracture morphologies of base metal, (f) EDS analysis of base metal.

The phenomenon of chromium (Cr) and manganese (Mn) segregating at grain boundaries, resulting in relatively lower concentrations within the austenite matrix, has been consistently observed in various studies [18]. This behavior aligns with the previously discussed findings. The preferential segregation of Cr and Mn at the grain boundaries is a well-documented characteristic of specific alloy systems. This can affect the mechanical properties, corrosion resistance, and other factors of the material. Multiple investigations have documented such segregation patterns, indicating their significance in the microstructural analysis of materials containing Cr and Mn [58]. The formation of these segregated phases at the grain boundaries of the heat-affected zone can lead to grain-boundary liquefaction and produce cracks that degrade the mechanical properties and corrosion resistance of the material [43]. The same color orientations shown in Fig. 3 represent the phase distributions in the underwater wet weld Fig. 3(b) shows that most of the peaks indicated by 5 and 6 grew along the boundary line. As shown in Fig. 3(a), alloy AH36 consisted of refined grains with random grain orientations in the region indicated by number 1. The formation of twin boundaries was observed in Region 3. The fine-grained part is close to the fusion boundary, as shown in Fig. 3(b) and apparent grain growth was observed in the HAZ, as shown by number 4 in Fig. 3(c). In addition, evidence of type-II grain boundaries parallel to the fusion line is shown in Fig. 3(e). It can be seen that the C-based welds and AH36 base metal have a body centered cubic structure.

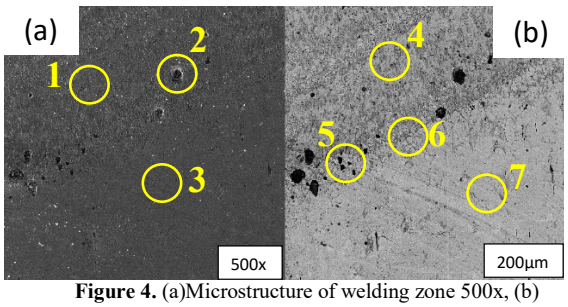

Figure 4. (a)Microstructure of welding zone 500x, (b) Microstructure of welding zone of 200µm.

The grain boundary type is closely related to the stress corrosion resistance of the grain boundaries. Typically, grain boundaries can be classified into low-angle boundaries (LABs, 2-15°) and high-angle grain boundaries (HABs, 15-180°). Fig. 4 shows that the grain boundaries in the base metal were composed of LABs and HABs, whereas very few LABs were observed in the weld zone and HAZ. This showed elemental migration from seawater to the HAZ and weld zone.

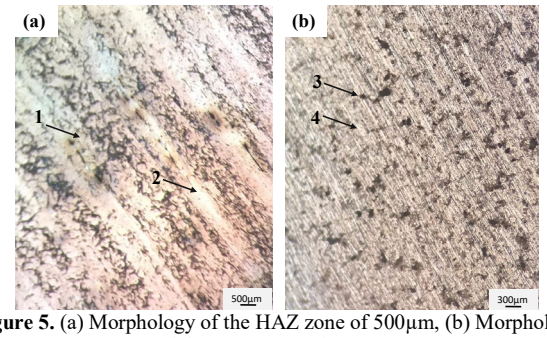

Figure 5. (a) Morphology of the HAZ zone of 500µm, (b) Morphology of the HAZ zone of 300µm.

Fig. 5 shows the microstructural characteristics of wet-welded joints. The weld metal (1) was completely austenite in structure, with equiaxed grains at the top of the welds (2) and columnar grains at the bottom of the welds (3). This phenomenon is closely related to the change in solidification mode from cellular to dendritic morphology. The solidification mode depends on the combined effects of the composition, temperature gradient, and solidification rate. The equiaxed grains in Fig. 5 (a) were observed at the ends of the welds, where the temperature gradient was shallow owing to arc extinction. Fig. 5 (b) shows the columnar grain formation due to the increased solidification rate for high-temperature gradients [32]. The direction of columnar grain growth in the carbon-based weld metal was consistent with the heat transfer direction.

3.2 Mechanical Performance

Compared with previous studies, grain size and inclusions were not the determining factors that improved the UTS of the weld metal (the average ultimate tensile strength). The difference solid-solution-forming elements reduce the strength of the solid- solution, primarily by reducing the resistance to the movement of dislocations, as shown in Fig. 6.

According to Roth [53] and Liang [54], the solid-solution strengthening effect owing to multiple alloying elements was determined using Equation 2, where i is the type of solute, k_i is the hardening coefficient for solute i, and c_i is the concentration of solute I (% at.).

$$\Delta\sigma=\sum_i [\![k_i \sqrt{(C_i)}]\!] \quad (2)$$

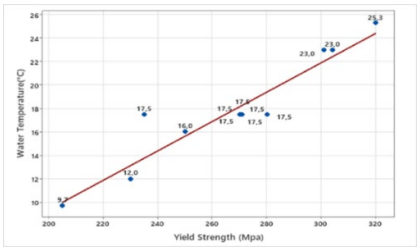

Figure 6. Multi-response optimization of water temperature and yield strength.

3.3 Optimisation Results with the Response Vertical Method

The RSM method modeled yield stress values obtained from tensile tests and seawater temperature, and is shown in the following equation:

$$\text{Yield Strength} = 223.164 + 5.118X_1 - 1.017X_2 + 0.053X1*X_2 - 0.065X_{22} - 0.034X_{22} \quad (3)$$

For the obtained equation to be compatible with the model, the three regression values expressing the model should be close to each other and have high values. In the model, predictive R^2 (0,7883), adjusted R^2 (0,9489), and total R^2 (0,9702) were found to be high and compatible. This value shows that the yield strength obtained by the model can be predicted with an error of 2.98%, even for experiments not performed at the studied weld current intensity (X_1) and seawater temperature (X_2). The obtained equation shows that seawater temperature significantly affects yield strength. The presence of the interactive term $X_1 \times X_2$ in the equation indicates that seawater temperature and weld current intensity jointly affect the yield strength of AH36. X_{12} and X_{22} in this equation indicate that a quadratic effect is possible. As a result of the modeling, two-dimensional and three-dimensional graphs were drawn for AH36 (Fig. 7a, b), relating the change in yield strength to the seawater temperature and weld current intensity.

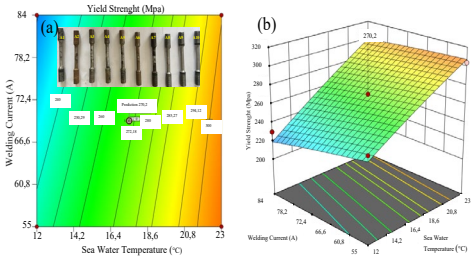

Figure 7. RSM optimization results.

3.4 Sea Water Elemental Composition

The P value was not measured in ICP-MS analysis and the results of this analysis are shown in Table 2. It is indicated with a negative sign. The values shown in Table 2 are unitless and represent the ratio (ppm) relative to each other.

After ICP-MS analyses were performed on the seawater samples after the weld, it was found that there was a multi-response optimization relationship with a high rate of 87.3% (R^2) between the Cr ratio change between the weld and seawater at different weld current values. This relationship was formulated as Cr=304,7-10,36X_2 + 0,0866X_{22} multi-response optimization equation. Thus, the difference in the Cr content in seawater can be predicted to a large extent in advance using the weld current values. No relationship was found between seawater temperature and Cr content in seawater.

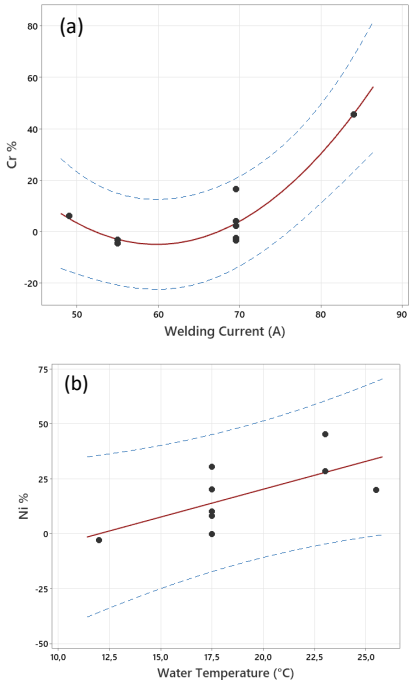

Figure 8. (a) Cr (%Wt)-Welding current relation, (b) Ni (%Wt)-Water temperature relation.

As shown in Fig. 8(a)-(b), ICP-MS analyses showed significant correlation with Cr, Ni and Mn values. ICP-MS analyses significantly correlated the Cr, Ni, and Mn values. It was observed that the changes in the Ni and Mn ratios of the weld parameters in seawater were not as highly correlated as those of Cr. It was observed that the change in the Ni ratio in seawater after welding was not related to the spring flow as in Cr, but to the change in the temperature of the seawater. However, this was a low correlation of 64.45% (R^2). This relationship was formulated using the multi-response optimization equation Ni=-30.3+2.54X1. Unlike Cr and Ni, the change in Mn content in seawater is related to seawater temperature and welding current values, but this relationship is as low as 65.74% (R^2). It is formulated with Mn=-70753+3990 X1+1095X2-58.9 X1 X2 (X1: Welding current, X2: Water temperature).

4 Conclusion

The main results of this study are as follows:

(1) The EDS spot analysis revealed predominant distribution of chromium (Cr) and manganese (Mn) within the base metal AH36, indicating higher concentrations compared to the weld metal. A notable gradient in chromium (Cr) diffusion was observed at the interface between the AH36 base metal and the adjacent weld metal, suggesting significant changes in distribution. Additionally, identification of Nb-rich phases through EDS analysis and the formation of chromium oxide (Cr_2O_3) under higher carbon content provided insights into the material's behavior. The presence of a block-shaped white phase rich in Cr and Mn was confirmed in the AH36 base metal, signifying specific elemental behavior and compound formation. These findings collectively contribute to understanding the microstructure and elemental composition intricacies of AH36 material under various conditions.

(2) A relationship between the changes in the seawater chemistry (i.e. Cr, Ni, and Mn ratios) and welding parameters was observed. The Cr ratio was directly related to the welding current, the Ni ratio was directly related to the seawater temperature, and the Mn ratio was directly associated with both the seawater temperature and welding current.

(3) It was observed that the HAZ region of the low-carbon alloy AH36 metal had a ferrite and austenite structure and irregular distribution, and the elemental change in this region was high according to EDS point analyses. These results show that the HAZ region had the highest element diffusion into seawater after welding.

(4) An absolute decrease in the yield strength value of AH36 metal after submarine welding was observed. The optimum yield strength was determined to be 270 MPa using RSM.

(5) It was determined that 87.3% of the diffusion into seawater during welding depends on the welding current so that the Cr element can be controlled before the target value of 0.06 ng/ml recommended by California Public for Cr6+. Thus, a mathematical model has been developed to mitigate the environmental damage caused by Cr element.

(6) With the findings obtained in this study, parameters such as determination of welding parameters, control of environmental impact, prediction of mechanical properties and productivity in underwater welding applications are determined. These results play an important role in improving quality, reducing environmental impact and improving efficiency in underwater welding applications.

Decleration

An ethics committee approval document is not required for this study.

References

[1] Chen, H., Guo, N., Zhang, X., Cheng, Q., Zhou, L., & Wang, G. (2020). Effect of water flow on the microstructure, mechanical performance, and cracking susceptibility of underwater wet welded Q235 and E40 steel. *Journal of Materials Processing Technology, 277, 116435.*

[2] Chen, H., Guo, N., Shi, X., Du, Y., Feng, J., & Wang, G. (2018). Effect of water flow on the arc stability and metal transfer in underwater flux-cored wet welding. *Journal of Manufacturing Processes,* 31, 103-115.

[3] Klett, J., Hecht-Linowitzki, V., Grünzel, O., Schmidt, E., Maier, H. J., & Hassel, T. (2020). Effect of the water depth on the hydrogen content in SMAW wet welded joints. *SN Applied Sciences,* 2, 1-14.

[4] Santos, V. R., Bracarense, A. Q., Pessoa, E. C. P., Marinho, R. R., Rizzo, F. C., Junior, R. C., & Monteiro, M. J. (2022). Development of oxyrutile low alloy ferritic electrode for wet welding. *Journal of Materials Research and Technology*, 21, 1223-1247.

[5] Santos, V. R., Bracarense, A. Q., Pessoa, E. C. P., Marinho, R. R., Rizzo, F. C., Nóbrega, A. F., ... & Rebello, J. M. A. (2021). Prediction of hydrogen cracking in the wet welding of structural steels with ferritic stick electrodes down to 20 m. *Journal of Materials Research and Technology*, 15, 5787-5802.

[6] Putri, E. D. W. S., Surojo, E., & Budiana, E. P. (2020). Current research and recommended development on fatigue behavior of underwater welded steel. *Procedia Structural Integrity,* 27, 54-61.

[7] Wang, J., Sun, Q., Hou, S., Zhang, T., Jin, P., & Feng, J. (2019). Dynamic control of current and voltage waveforms and droplet transfer for ultrasonic-wave-assisted underwater wet welding. *Materials & Design,* 181, 108051.

[8] Luna, L. E. R., Bracarense, A. Q., Pessoa, E. C. P., Costa, P. S., Guerrero, G. A., & Reyes, A. E. S. (2021). Effect of the welding angle on the porosity of underwater wet welds performed in overhead position at different simulated depths. *Journal of Materials Processing Technology*, 294, 117114.

[9] Wang, J., Sun, Q., Jiang, Y., Zhang, T., Ma, J., & Feng, J. (2018). Analysis and improvement of underwater wet welding process stability with static mechanical constraint support. *Journal of Manufacturing Processes,* 34, 238-250.

[10] Küçükömeroğlu, T., Aktarer, S. M., & Çam, G. (2019, September). Investigation of mechanical and microstructural properties of friction stir welded dual phase (DP) steel. In IOP Conference Series: *Materials Science and Engineering* (Vol. 629, No. 1, p. 012010). IOP Publishing.

[11] Küçükömeroğlu, T., Aktarer, S. M., İpekoğlu, G., & Çam, G. (2018). Mechanical properties of friction stir welded St 37 and St 44 steel joints. *Materials Testing*, 60(12), 1163-1170.

[12] Çam, G. (2005). Friction stir welding (FSW)-A novel welding technology developed for Al-Alloys. *Mühendis ve Makina (Engineer and Machinery)*, 46(541), 30-39.

[13] Ahmed, M. M., Seleman, M. M. E. S., Fydrych, D., & Gürel, Ç. A. M. (2023). Review on friction stir welding of dissimilar magnesium and aluminum alloys: Scientometric analysis and strategies for achieving high-quality joints. *Journal of Magnesium and Alloys*.

[14] Khaliq, U. A., Muhamad, M. R., Yusof, F., Ibrahim, S., Isa, M. S. M., Chen, Z., & Çam, G. (2023). A review on friction stir butt welding of aluminum with magnesium: A new insight on joining mechanisms by interfacial enhancement. *Journal of Materials Research and Technology.*

[15] Küçükömeroğlu, T., Aktarer, S. M., İpekoğlu, G., & Çam, G. (2018). Microstructure and mechanical properties of friction-stir welded St52 steel joints. *International Journal of Minerals, Metallurgy, and Materials,* 25, 1457-1464.

[16] Şenol, M., & Çam, G. (2023). Investigation into microstructures and properties of AISI 430 ferritic steel butt joints fabricated by GMAW. *International Journal of Pressure Vessels and Piping,* 202, 104926.

[17] Ezer, M. A., & Çam, G. (2022). A study on microstructure and mechanical performance of gas metal arc welded AISI 304 L joints. *Materialwissenschaft und Werkstofftechnik*, 53(9), 1043-1052.

[18] Serindağ, H. T., & Çam, G. (2023). Characterizations of microstructure and properties of dissimilar AISI 316L/9Ni low-alloy cryogenic steel joints fabricated by gas tungsten arc welding. *Journal of Materials Engineering and Performance,* 32(15), 7039-7049.

[19] Serindağ, H. T., Tardu, C., Kirçiçek, İ. Ö., & Çam, G. (2022). A study on microstructural and mechanical properties of gas tungsten arc welded thick cryogenic 9% Ni alloy steel butt joint. *CIRP Journal of Manufacturing Science and Technology,* 37, 1-10.

[20] Serindağ, H. T., & Çam, G. (2021, February). Microstructure and mechanical properties of gas metal arc welded AISI 430/AISI 304 dissimilar stainless steels butt joints. *In Journal of Physics: Conference Series* (Vol. 1777, No. 1, p. 012047). IOP Publishing.

[21] Shi, C., Cao, J., Han, S., Hu, K., Bian, L., & Yao, S. (2021). A review of polymetallic mineralization in lower Cambrian black shales in South China: Combined effects of seawater, hydrothermal fluids, and biological activity. *Palaeogeography, Palaeoclimatology, Palaeoecology,* 561, 110073.

[22] Balaram, V., Copia, L., Kumar, U. S., Miller, J., & Chidambaram, S. (2023). Pollution of water resources and application of ICP-MS techniques for monitoring and management–A comprehensive review. *Geosystems and Geoenvironment,* 100210.

[23] Meng, X., Jin, X., Li, X., Chu, F., Zhu, J., Wang, Y., & Zhou, P. (2022). Subseafloor mineralization related to the shallow seawater-hydrothermal circulation system in the Longqi hydrothermal field, Southwest Indian Ridge (49.6 E): Evidence from in situ trace element and sulfur isotope compositions of pyrite varieties. *Ore Geology Reviews*, 145, 104914.

[24] Soriano, E., Pastor, A., & de la Guardia, M. (2020). Multielemental determination of trace mineral elements in seawater by dynamic reaction cell inductively coupled plasma-mass spectrometry after Al (OH) 3 coprecipitation. *Microchemical Journal,* 157, 104864.

[25] Dey, M., Ghosh, B., & Giri, T. K. (2020). Enhanced intestinal stability and pH sensitive release of quercetin in GIT through gellan gum hydrogels. *Colloids and surfaces B: Biointerfaces,* 196, 111341.

[26] Wei, Y., Yuan, C., Xu, X., Chen, X., Ren, Z., Gui, X., ... & Cao, X. (2022). Colloid formation and facilitated chromium transport in the coastal area soil induced by freshwater and seawater alternating fluctuations. *Water Research,* 218, 118456.

[27] Li, J., Chen, H., Liu, W., Ding, X., Zhong, R., & Yu, C. (2022). Copper mobilization via seawater-volcanic rock interactions: New experimental constraints for the formation of the iron oxide Cu-Au (IOCG) mineralization. *Geochimica et Cosmochimica Acta,* 330, 209-229.

[28] Vashishtha, P., Wattal, R., Pandey, S., & Bhadauria, N. (2022). Problems encountered in underwater welding and remedies-a review. *Materials Today: Proceedings,* 64, 1433-1439.

[29] Tomków, J., Landowski, M., Fydrych, D., & Rogalski, G. (2022). Underwater wet welding of S1300 ultra-high strength steel. *Marine Structures,* 81, 103120.

[30] Li, H., Liu, S., Sun, F., Ma, Q., Ji, H., Liu, H., & Chen, H. (2022). Improvement of microstructure and mechanical properties for underwater wet 16Mn/304L dissimilar steel welded joints assisted by presetting butter layer. *Materials Today Communications,* 33, 104259.

[31] Li, H., Liu, S., Sun, F., Yu, L., Wang, J., Wang, Z., ... & Lei, Y. (2022). Preliminary investigation on underwater wet welding of Inconel 625 alloy: microstructure, mechanical properties and corrosion resistance. *Journal of Materials Research and Technology,* 20, 2394-2407.

[32] Zhang, M., Han, Y., Jia, C., Zheng, Z., Li, H., & Wu, C. (2022). Improving the microstructures and mechanical properties with nano-Al2O3 treated wire in underwater submerged arc welding. *Journal of Manufacturing Processes,* 74, 40-51.

[33] Amaral, E. C., Moreno-Uribe, A. M., & Bracarense, A. Q. (2021). Effects of PTFE on operational characteristics and diffusible H and O contents of weld metal in underwater wet welding. Journal of Manufacturing Processes, 61, 270-279.

[34] Li, X., Zhang, Z., Peng, Y., Yan, D., Tan, Z., Zhou, Q., ... & Zhou, M. (2022). Microstructure and mechanical properties of underwater friction stir welding of CNT/Al-Cu-Mg composites. *Journal of Materials Research and Technology,* 18, 405-415.

[35] Philip, A. J. P., Fjelldal, P. G., Remø, S. C., Selvam, C., Hamre, K., Espe, M., ... & Sissener, N. H. (2022). Dietary electrolyte balance of Atlantic salmon (Salmo salar) freshwater feeds: Impact on osmoregulation, mineral metabolism and performance in seawater. *Aquaculture*, 546, 737305.

[36] Bar-Or, D., Rael, L. T., Bar-Or, R., Thomas, G. W., Slone, D. S., Melamed, I., & Craun, M. L. (2006). Severe systemic immune response syndrome, low plasma paraoxonase activity, and a new albumin species in a traumatized patient with Gaucher's disease. *Clinica chimica acta,* 374(1-2), 135-139.

[37] Wang, Z., Zhang, Y., Wang, T., Hao, L., Lin, E., Chen, Y., ... & Zhang, Z. (2023). Organic flux synthesis of covalent organic frameworks. *Chem*, 9(8), 2178-2193.

[38] Pereira, P. L., Arnold, D., de Baère, T., Gomez, F., Helmberger, T., Iezzi, R., ... & Taieb, J. (2020). A multicentre, international, observational study on transarterial chemoembolisation in colorectal cancer liver metastases: Design and rationale of CIREL. *Digestive and Liver Disease,* 52(8), 857-861.

[39] Papageorgiou, N., Falconer, D., Wyeth, N., Lloyd, G., Pellerin, D., Speechly-Dick, E., ... & Bhattacharyya, S. (2020). Effect of tricuspid regurgitation and right ventricular dysfunction on long-term mortality in patients undergoing cardiac devices implantation:> 10-year follow-up study. *International Journal of Cardiology,* 319, 52-56.

[40] Chan, Q., Wang, F., Shi, L., Ren, X., Ren, T., & Han, Y. (2022). Effects of chronic dietary hexavalent chromium on bioaccumulation and immune responses in the sea cucumber Apostichopus japonicus. *Comparative Biochemistry and Physiology Part C: Toxicology & Pharmacology,* 252, 109218.

[41] Wise Sr, J. P., Wise, S. S., Holmes, A. L., LaCerte, C., Shaffiey, F., & Aboueissa, A. M. (2010). The cytotoxicity and genotoxicity of hexavalent chromium in Steller sea lion lung fibroblasts compared to human lung fibroblasts. *Comparative Biochemistry and Physiology Part C: Toxicology & Pharmacology,* 152(1), 91-98.

[42] Li, H., Liu, S., Sun, F., Ma, Q., Ji, H., Liu, H., & Chen, H. (2022). Improvement of microstructure and mechanical properties for underwater wet 16Mn/304L dissimilar steel welded joints assisted by presetting butter layer. *Materials Today Communications,* 33, 104259.

[43] Zhang, X., Guo, N., Xu, C., Du, Y., Chen, B., & Feng, J. (2019). Influence of CaF2 on microstructural characteristics and mechanical properties of 304 stainless steel underwater wet welding using flux-cored wire. *Journal of Manufacturing Processes,* 45, 138-146.

[44] Sultana, M. N., & Dhar, N. R. (2023). RSM design-based hybrid approach to multi-response optimization in milling Ti-6Al-4 V alloy: A comparative study. *Materials Today: Proceedings.*

[45] Şenol, H., Erşan, M., & Görgün, E. (2020). Optimization of temperature and pretreatments for methane yield of hazelnut shells using the response surface methodology. *Fuel*, 271, 117585.

[46] Wang, J., Sun, Q., Pan, Z., Yang, J., & Feng, J. (2019). Effects of welding speed on bubble dynamics and process stability in mechanical constraint-assisted underwater wet welding of steel sheets. J*ournal of Materials Processing Technology,* 264, 389-401.

[47] Li, H., Liu, D., Yan, Y., Guo, N., Liu, Y., & Feng, J. (2018). Effects of heat input on arc stability and weld quality in underwater wet flux-cored arc welding of E40 steel. *Journal of Manufacturing Processes*, 31, 833-843.

[48] Wang, J., Sun, Q., Zhang, S., Wang, C., Wu, L., & Feng, J. (2018). Characterization of the underwater welding arc bubble through a visual sensing method. J*ournal of Materials Processing Technology,* 251, 95-108.

[49] Chen, H., Guo, N., Huang, L., Zhang, X., Feng, J., & Wang, G. (2019). Effects of arc bubble behaviors and characteristics on droplet transfer in underwater wet welding using in-situ imaging method. *Materials & Design*, 170, 107696.

[50] Pell, A., Kokkinis, G., Malea, P., Pergantis, S. A., Rubio, R., & López-Sánchez, J. F. (2013). LC–ICP–MS analysis of arsenic compounds in dominant seaweeds from the Thermaikos Gulf (Northern Aegean Sea, Greece). *Chemosphere*, 93(9), 2187-2194.

[51] Rodriguez-Cea, A., Arias, A. L., de la Campa, M. F., Moreira, J. C., & Sanz-Medel, A. (2006). Metal speciation of metallothionein in white sea catfish, Netuma barba, and pearl cichlid, Geophagus brasiliensis, by orthogonal liquid chromatography coupled to ICP-MS detection. *Talanta*, 69(4), 963-969.

[52] Erkan, N., & Özden, Ö. (2007). Proximate composition and mineral contents in aqua cultured sea bass (Dicentrarchus labrax), sea bream (Sparus aurata) analyzed by ICP-MS. *Food chemistry,* 102(3), 721-725.

[53] Lenz, C., Behrends, T., Jilbert, T., Silveira, M., & Slomp, C. P. (2014). Redox-dependent changes in manganese speciation in Baltic Sea sediments from the Holocene Thermal Maximum: An EXAFS, XANES and LA-ICP-MS study. *Chemical Geology*, 370, 49-57.

[54] Elseblani, R., Cobo-Golpe, M., Godin, S., Jimenez-Lamana, J., Fakhri, M., Rodríguez, I., & Szpunar, J. (2023). Study of metal and organic contaminants transported by microplastics in the Lebanese coastal environment using ICP MS, GC-MS, and LC-MS. *Science of The Total Environment,* 887, 164111.

[55] Abdelaal, A., Sarayloo, M., Nims, D. K., Mohammadian, B., Heil, J., & Sojoudi, H. (2022). A flexible surface-mountable sensor for ice detection and non-destructive measurement of liquid water content in snow. *Cold Regions Science and Technology,* 195, 103469.

[56] Sarkar, C., Spada, N., Xu, S., Shafer, M. M., & Hyslop, N. P. (2023). An inter-laboratory comparison of elemental loadings of PM2. 5 samples using energy-dispersive XRF and magnetic-sector ICP-MS. *Atmospheric Environment, 293,* 119463.

[57] Ramkumar, D. H. S., & Kudchadker, A. P. (1990). Phase equilibria of water+ γ-butyrolactone system. *Fluid phase equilibria*, 55(1-2), 207-215.

[58] Terán, G., Cuamatzi-Meléndez, R., Albiter, A., Maldonado, C., & Bracarense, A. Q. (2014). Characterization of the mechanical properties and structural integrity of T-welded connections repaired by grinding and wet welding. M*aterials Science and Engineering:* A, 599, 105-115.